Summer 2024

Resonant Ultrasound Spectroscopy(RUS) for Material Characterization of Metal AM Parts

Malik Marks

RESONANT ULTRASOUND SPECTRCOCOPY FOR MATERICAL CHARACTERIZATION OF METAL AM PARTS

by

MALIK MARKS

PROFESSOR HOSSEIN TAHERI

Additive manufacturing (AM) has revolutionized the manufacturing industry by offering flexibility, customization, and rapid prototyping capabilities. However, ensuring the quality and reliability of AM parts remains a significant challenge due to variations in material properties and process parameters. The NDE method used in this study is Resonant Ultrasound Spectroscopy (RUS). This method was used to evaluate and understand its ability to detect internal voids and defects. Dog-bone samples were made using the 316L stainless steel alloy which were fabricated by powder bed fusion (PBF) AM technique at different processing conditions and post processing conditions. These samples were tested to find their mechanical properties and how the process parameters affected these properties. A correlation study was done using Pearson's and scan speed had been shown to have the most influence of the mechanical properties. Next, RUS was used to see if it could distinguish the three different groups from one another. Based on the Z-Scores RUS was able to distinguish the groups from one another and based on the Z-score plot there is a clear separation between the groups. A correlation was established between the RUS and the mechanical properties and based on these results RUS data correlates well with mechanical properties tested except for the fatigue testing. This r value was below .5. Lastly, FEM was used to compare the actual change in frequency measured by RAM to the change in frequency spectrum using FEM. Based on the numerical results FEM was also able to distinguish between the groups.

INDEX WORDS: NDE 4.0, Additive Manufacturing, RUS, NDT-RAM, AM, Material Characterization, Resonance

RESONANT ULTRASOUND SPECTRCOCOPY FOR MATERICAL CHARACTERIZATION OF METAL AM PARTS

by

MALIK MARKS

B.S., Georgia Southern University, 2021

M. Ed., Georgia Southern University, 2024

RESONANT ULTRASOUND SPECTRCOCOPY FOR MATERICAL CHARACTERIZATION OF METAL AM PARTS

by

MALIK MARKS

Major Professor:	Hossein Taheri
Committee:	Haijun Gong
Committee:	Kamran Kardel

Electronic Version Approved:
July 2024

TABLE OF CONTENTS

Page

LIST OF TABLES

LIST OF FIGURES

Chapter 1
INTRODUCTION

1. Literature Review

Due to its ability to print very complex parts with relative ease, metal additive manufacturing (AM) is increasing in popularity[1]. Unlike traditional manufacturing which consists of subtracting material through either drilling, cutting, etc., additive manufacturing (AM) creates a part by adding new material layer by layer. However, there are numerous parameters that can directly influence the mechanical property and quality of the as-built parts including laser power, hatch size, scan speed, etc., and defects are common in parts thus affecting its' mechanical properties[2–5]. These inconsistencies in material property have led to low reliability in AM parts, which limits its adoption into many industries outside of aerospace, automotive, medical, and the defense sector[6]. Thus, providing a need and interest in applying new nondestructive evaluation (NDE) for part quality evaluation.

Part quality testing in additive manufacturing is an integral part in the evaluation process. Non-destructive testing is a way to evaluate the quality and collect data of a structure or parts without damaging the object being tested. It is commonly used to evaluate defects, cracks, or porosity that led to low quality materials. There are many NDT techniques (eddy current, XCT, ultrasonic testing, etc.) The technique chosen is based on several different criteria: size and type of defect, geometry of sample, complexity, application needed, etc. For example, XCT or x-ray computed topography is mainly used to look at the porosity of the sample, but it is very costly and usually coupon of the sample is needed due to the poor resolution if sample size is too thick[7,8]. Ultrasonic testing or UT is a very powerful technique that can study defects in the

part, but like XCT very costly and time consuming. Also, when defects are given in the planar direction parallel to the trajectory of ultrasonic waves it may not detect the defect[9]. Eddy current testing is mainly used for shallow or near surface cracks but requires advanced analytics and very stable conditions in the material to avoid unwanted signals[9].

In this study Resonance Ultrasound Spectroscopy (RUS) will be used to explore its ability to detect defected parts. Unlike other NDE techniques, RUS is a very accurate, simple technique, and inexpensive. RUS is an attractive technique because of its ability to test parts with complex geometry very easily and quickly. This technique measures the resonance frequency response of a sample following an excitation.

Traditionally, RUS was mainly used to obtain the elastic properties of simple geometric samples using the theory of elasticity. To accurately obtain the elastic constants, the modes excited need to be correctly identified and matched with the frequencies in the forward problem[10]. Once the natural frequencies are obtained, then one must apply nonlinear inversion technique to find the elastic constants from the frequency spectrum [11]. Due to the relatively ease of this technique, advancement in the theory and technology, RUS has been used to find the elastic constants of many materials[12]. For example, wood[13], has been used in the medical field for biological materials such as bone tissue and human enamel[14,15]. Also, can be used to record elastic constant measurements at high or low temperature, and high pressures[16,17].

Outside of elastic tensor measurements, RUS with the combination of FEA has been used to analyze defects in parts. For specimens with known geometry and elastic constants, FEA was used to identify the location and depth of large defects based on the numerical resonant frequencies calculated by the model[18,19]. However, these studies were of large defects and the predicted numerical results were not compared to experimental results. In Flynn and Radovic

study, they compared the experimental and FEA generated frequency spectrum of before notched and notched samples. Their finding concluded they were able to not only identify if an object has a defect, but the size and location of the defect within average error less than 5 percent[20]. However, the of the size defects(.67mm-2.35mm) were relatively large, compared to additive manufacturing defects which can be significantly smaller[21,22].

In the AM field, RUS has mainly been used for part qualification and material characterization. In Ross et al. research they utilized this technique to obtain the crystalline orientation and match the resonance frequencies of the textured and recrystallized state of the material to assess the grain structure evolution in nickel alloy[23]. They were able to demonstrate RUS ability to detect part to part microstructure changes between AM components[23]. In Dababneh et al they were able to accurately assess different resonance frequencies for different deposition regions, before and after in the interruption line in wire arc manufacturing (WAAM) using RUS[24].

Due to the relatively easiness and quickness of the technique to test more geometrically complex parts[25], it has been used to evaluate AM lattice structures. In Ibrahim et al, they used acoustic resonance testing and FEA to test the effective modulus and relative density of bulk and lattice samples[26]. They found that there was good agreement between the effective modulus acoustic resonance and FEA results, however there was more of a deviation for the relative density results. They attributed this deviation to the loose powder adhesion effect[26]. Like Ibrahim et al, McGuigan et al used RUS combined with FEA to evaluate lattice structures. However, they used the technique for part qualification of different lattices. They explored RUS ability to not only detect the defects, but potentially to distinguish between the number of

missing struts. Using RUS and FEM, Mcguigan was able to distinguish between pristine part and parts with missing structures, but data on the number of missing struts could not be inferred[27].

RUS provides a fair amount of data which can be used for different statistical analysis and machine learning techniques to aid in part quality classification. For example, in Obaton et al study, used RUS in tandem with regularized linear discriminant analysis, combined with adaptive sampling and normalization, to classify the number of missing struts, which FEM was unable to in Mcguigan's study. They were able to classify the defects with 100 percent training accuracy and a training model with 81 percent accuracy[28]. In a similar study, they used three different statistical techniques, z-score, supervised, and unsupervised models to analyze the RUS data on a batch of samples that were supposedly identical. They found that each method was able to differentiate the parts from one another and the highest performing in terms of mean accuracy and sensitivity was the Naïve Bayes model[29]. In Todd's et al study, they investigated using RUS and linear regression to predict the mechanical properties of Ti-6Al-4v manufactured by SLM. They used as-built samples and annealed samples. They concluded that resonant peaks in both sets can be used to predict the ultimate tensile strength, but there is little evidence for the other mechanical properties, yield strength, young's modulus, strain, reduction in area[30].

Although RUS looks promising as an inspection technique for AM parts, there is very limited research on correlating the RUS data to the mechanical properties of a sample. The goal of this work is to test RUS ability to detect defects in AM made samples and establish a correlation between the RUS and the mechanical properties. Three samples with different process parameters were manufactured. One set of samples, the control group, were made with optimal process parameters of the machine. One set of samples with low laser power and the other set with a lower scan speed. Another part of this project is to compare the FEA spectrum

response of all three groups to the experimental response. The long-term goal of this novel approach study is to provide an innovative inspection technique to characterize additive manufactured parts and provide a relationship between the structure and the property of the parts.

Chapter 2
EXPERIMENTAL METHODS

2.1 D.O.E

A One-Way ANOVA test was used to estimate the sample size needed to be manufactured for this experiment. This test is a technique that determines if there is statistical difference between two or more independent groups. To perform the sample size estimation the parameters needed for the power analysis are standard deviation, number of groups, differences, significance level, and power. Table 1 Table 2 show the parameters used in this study to conduct the power analysis. Table 1 shows the 6 different sample categories and their corresponding process or post process condition. Table 2 shows the expected experimental data for each material test and these numbers were chosen based on a previous experiment done before [25]. The power level chosen was .95, meaning there is a 5 percent chance we accept the null hypothesis. The statistical significance level chosen was .005. The power analysis was done for each test independently and the results are shown in Figure 1-3. The estimated total samples needed were 63, but due to the high sample size of the fatigue test and low sample size for the tensile test, a new number was calculated which is 12 samples for each group which in total is 72 samples.

Table 1: Variables and Description

	Sample Category	Manufacturing and Post-Process Conditions
	Group A	Optimum manufacturing process
	Group B	Samples manufactured at low laser power
	Group C	Samples manufactured at lower printing speed
	Group AH	A+ heat treatment
	Group BH	B+ heat treatment
	Group CH	C+ heat treatment

Table 2: Testing Parameters and Values

Variable	Material test	Typ. Value	Typ. (St. dev)	Max diff.
Material Testing				
	RUS--Resonance Frequency	40 (kHz)	5 (kHz)	10 (kHz)
	Tensile Strength	1100 (MPa)	20 (MPa)	250 (MPa)
	Fatigue Strength/Cycle	5500	1500	1500
	Metallography (% of porosity)	0.02	0.004	0.01
	Hardness	5 (GPa)	1 (GPa)	2 (GPa)

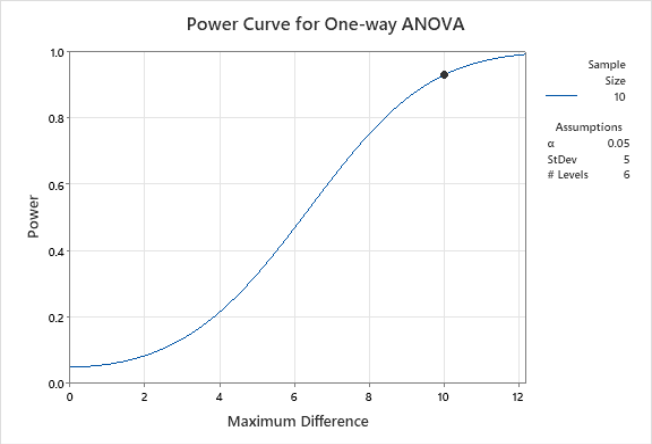

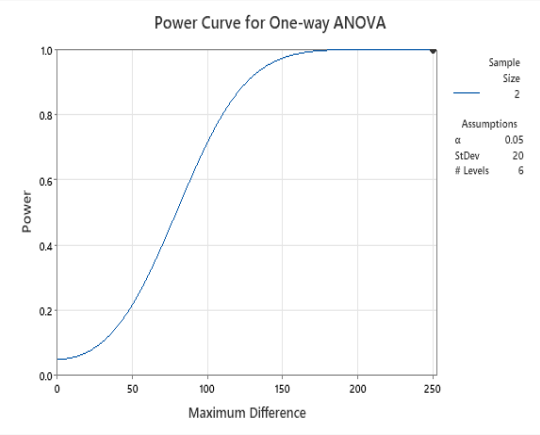

Figure 1 : Left side is ANOVA RUS results, and the right side is ANOVA tensile strength results.

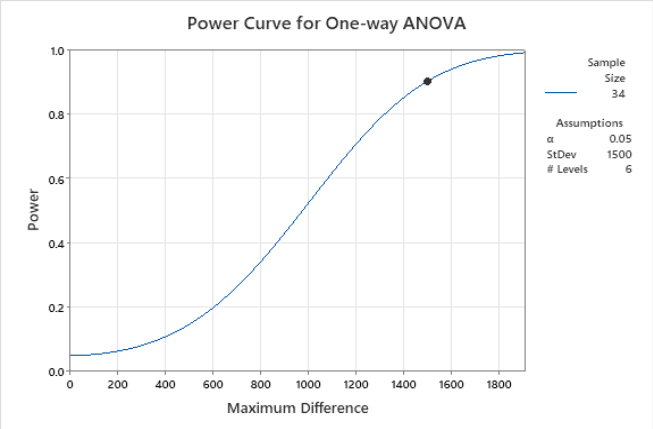

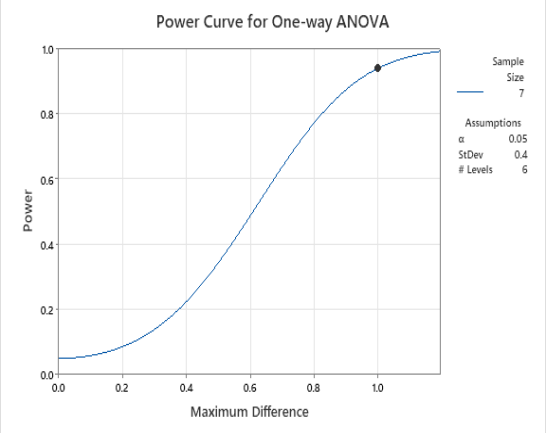

Figure 2 : Left side is ANOVA fatigue results and, the right side is ANOVA metallography results.

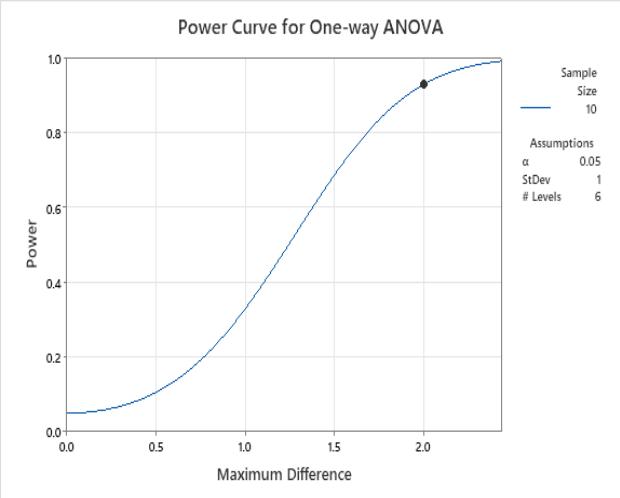

Figure 3:ANOVA hardness results.

2.2 Sample Fabrication

Samples were fabricated in a dog-bone shape according to ASTM E8 standard. The cross-section area of the samples in the gauge length area was 6x6mm. The Laser Powder Bed Fusion (LPBF) method was used to manufacture samples from stainless steel 316L alloy powder and the powder size used was 45 ±15 microns. Samples were fabricated at the different processing parameters as listed in Table 3. As previously discussed, group A was made with the

optimal parameters. Group B was manufactured with low laser power to introduce defects in the part due to lack of fusion or inadequate melting of the powder[31]. Group C was made with low scan speed to increase the cooling rate, thus also creating defects in the sample[32]. Table 4 shows the build report of the parts.

Table 3: Process Parameters

Group	Laser Power	Printing Speed
A, AH	225 W	1000 m/s
B, BH	195 W	1000m/s
C, CH	225 W	750m/s

Table 4: Build Report

Group	Build Time	Build height
A, AH	35 hrs. 55min	95.379mm
B, BH	39 hrs. 41min 20s	95.379mm
C, CH	39 hrs. 41min 20s	95.379mm

The parts were printed with the Farsoon FS217 Powder Bed Fusion machine which is shown in Figure 4. The printed parts just taken out of the build plate are shown in Figure 5. The parts were removed from the build plate, the supports were taken out, and a bit of post-processing was done to get the parts the same length for the RUS test, as geometry is an important variable in the RUS test. Any inconsistency between the samples geometry can negatively affect the results[33]. A mill was used to do the post-processing. The parts were aligned against the stock and the machine was zeroed in the x-axis. Figure 7 shows some samples of the parts after post-processing.

Figure 4 Farsoon Powder bed Fusion.

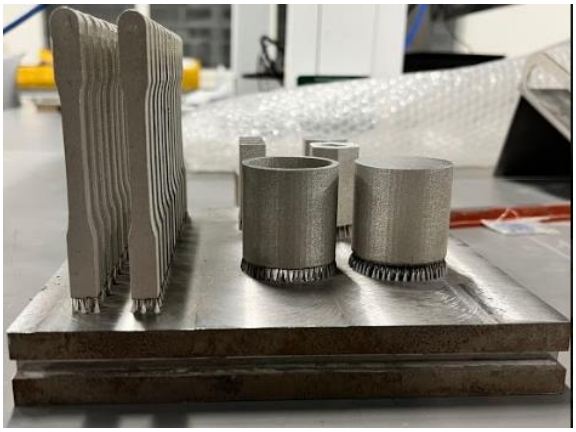

Figure 5: A, AH, B, BH, C, CH groups connected to build plate.

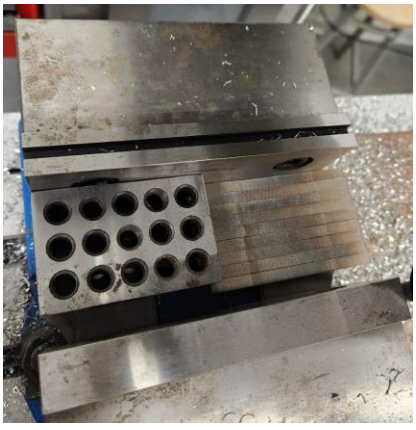

Figure 6: On the left side is machine used and right side is the setup.

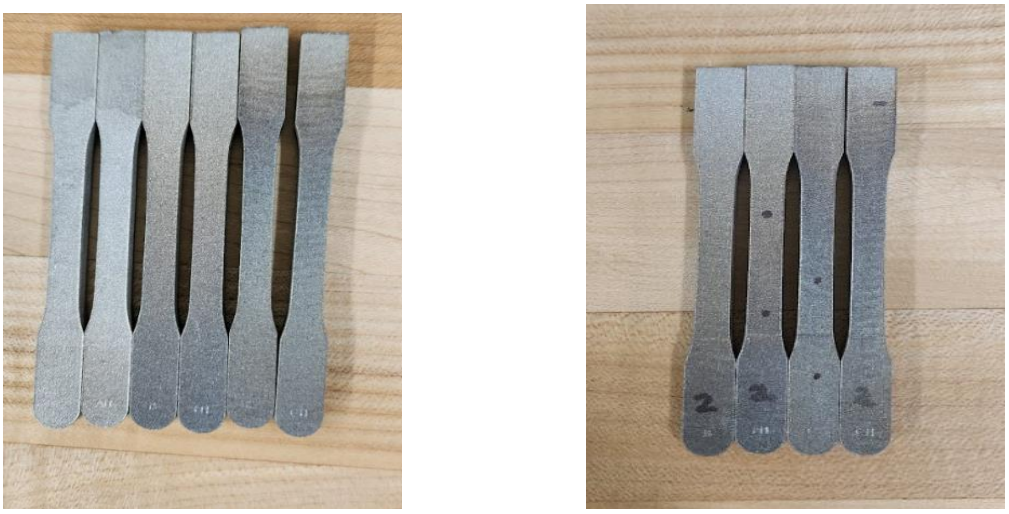

Figure 7: One sample from each group post-processing.

2.3 Heat Treatment Process

The groups with the letter (H) were heat -treated. Post-process heat treatment was not only used to test the feasibility of RUS in differentiating heat-treated parts from non-heat-treated parts, but also used because it has been known to alter the mechanical properties, grain size, and microstructure of the part[34,35]. These alterations can improve certain properties i.e. ductility of the material based on the heat treatment process used. The goal of this heat treatment was to improve the ductility, which would make the material softer, because of this an annealing heat treatment was used. Annealing helps reduce the hardness and the internal stresses of the part[36]. To achieve this samples were put into stainless steel bags to minimize surface oxidation, then put into the Sentro tech 1700C furnace. The samples were annealed at 1000 °C for 2 hours under an air atmosphere, then the furnace cooled for 4 hours. This temperature and hold time were chosen based on a previous study [37]. They were able to increase the elongation from 30 % to 54 %. In Figure 8, shows the heat treatment process used for this study.

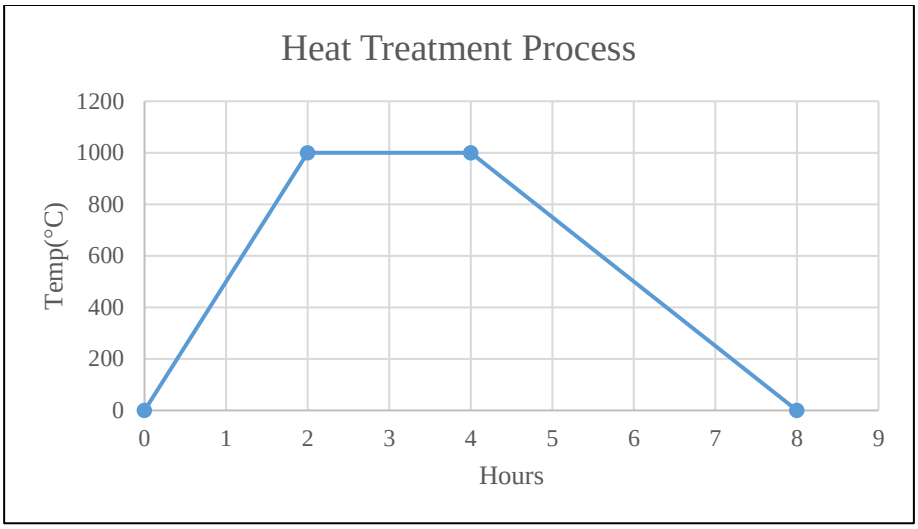

Figure 8: Heat Treatment Process

2.4 Density

The different process parameters changes are known to negatively affect the structural integrity of the part. These changes can generate more porosity or cracks in the part, which can affect the density. To assess the effect of the process parameters on the part quality, density measurements were taken of each sample in the non-heat-treated groups. The heat-treated samples were not measured, because the heat treatment process chosen has no effect on the density of the part. A total 11 samples from each group were weighed in grams using a digital scale and the volume was taken using the Archimede's method. All testing was done at around room temperature and repeated twice for each sample.

2.5 Tensile and Fatigue Test

Fatigue and tensile tests were done on the samples to acquire the yield strength, ultimate tensile strength, strain, and the fatigue life. These material properties have been shown to be influenced by the different process parameters, like change in laser power, speed, etc. Post heat treatment can have an effect as well on these material properties. These destructive tests were

used to evaluate how the process parameters listed in Table 3 would affect the mechanical properties of the sample.

Tensile tests were carried out according to ASTME8 standard. Tensile tests were conducted at room temperature using an MTS 810 Material Test System Servo-hydraulic system shown in Figure 9 with a constant crosshead velocity at 2mm/min until failure. A total of 3 samples were tested for each group.

Fatigue tests were performed according to ASTM E466 standard. Axial force-controlled fatigue test was used to obtain the fatigue life of the samples using a 10 Hz sinusoidal waveform under load control until the sample failed. The fatigue test was performed at R=0.1, which corresponds to the minimum stress being .1 times the maximum stress for each stress level. These tests were carried out in low cycle fatigue range (about $<10^4$ cycles) and high cycle fatigue range ($>10^5$ cycles). Experiments were performed at fixed stress levels based on the tensile test results (ex. 400, 300, and 250 MPa).

Figure 9: MTS Machine used for tensile and fatigue testing.

2.6 Nanoindentation

Nanoindentation technique is used to measure the mechanical properties of materials. The two main mechanical properties are the hardness(H) and modulus of elasticity(E). These properties are estimated from the load (P) versus displacement(h) measurement data recorded during the test. This was used to assess how the process parameters and the heat treatment will affect these two mechanical properties.

Two samples from each group, one sectioned in the x-direction and y-direction, (for a total of 12 samples) were grinded to obtain a flat surface and polished using two different polishing pads and .3um diamond solution agent, until a mirror-like surface was obtained. Testing was done with the Vickers indenter with a max load of 75mN, loading and unloading rate of 150mN/min, and a dwell time of 1.5s. The poison's ratio was set to .3 for stainless steel

316L alloy. Each sample was indented in a matrix of 5 x 6 points separated by 50um to avoid overlap. Figure 10 shows the NHT2 NANOINDENTER (Anton Paar, USA) and sample setup in the instrument.

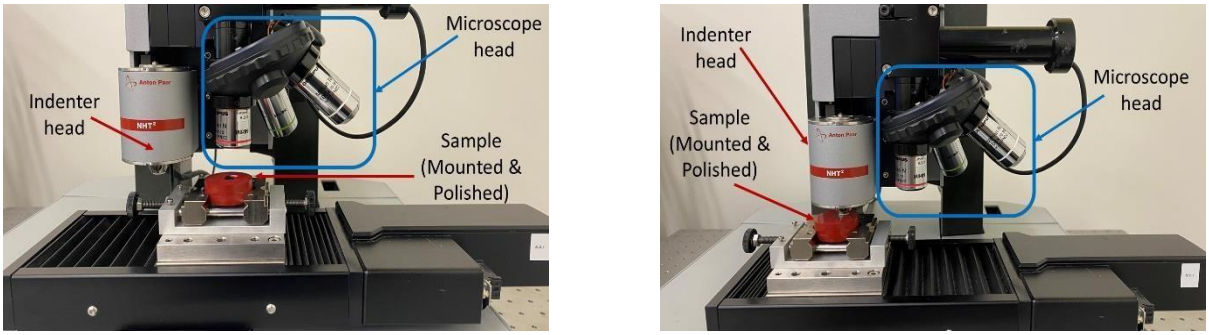

Figure 10 : The NANOINDENTER instrument under the microscope head of the instrument and indenter head of instrument.

2.7 RUS Experimental Setup

Differences in geometry, mass, stiffness, microstructure changes, defects, etc. can have significant impact on a part's resonance frequencies[38]. Like previously discussed, RUS is known to be sensitive to these changes. In a rather fast and simple test the frequencies of a single part can be known. These frequencies can be used to evaluate the modulus of the part or compare them to a control group. In the case of this study the resonance frequencies will be compared to a control group. The variations of the resonance frequencies mainly include the shifts in harmonics/resonance peaks and the number of harmonics/resonance peaks. These are good indicators for changes of the structural integrity of the samples.

The experimental tests were conducted by Weaver NDT using an NDT-RAM Resonant Ultrasound Spectrometer system by Modal Shop. Figure 11 shows the setup and schematic for RUS. The setup consists of a mic to record the signals, an impact hammer to act as the excitation device, an amplifier, and a DAQ system to record the data. Each part was gently tapped against

the modal hammer which is shown in Figure 11. The samples were excited, and the frequencies of each part were collected.

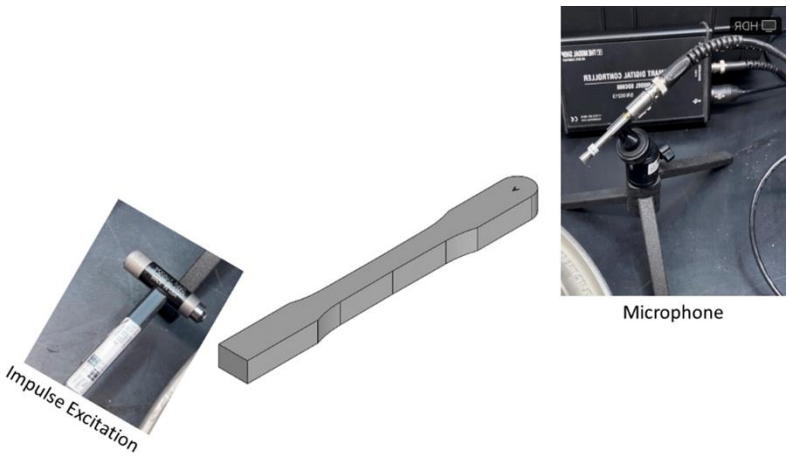

Figure 11: Experimental RUS setup by Weaver NDT

2.8 Finite Element Analysis

The FEA software used to perform the numerical simulations was done using COMSOL Multiphysics 6. For the simulation, the sample geometry was imported from SOLIDWORKS to COMSOL as an STL file. The dimensions were adjusted slightly to match the dimensions of the physical sample due to the machining of the samples after printing and removal from the build plate. The mesh was automatically generated by COMSOL using the physics-controlled mesh option. The option chosen was the 'extra fine' mesh after sensitivity analysis test was done and a less than 1 percent difference was found between using the finer mesh options, to avoid computational times. The smallest size was .133mm and maximum element size was 3.11mm. The simulations were done using COMSOL's Solid Mechanics module assuming a homogenous

and linear elastic material and Table 2, shows the different material properties used for each sample. These material properties were used based on the density and nanoindentation results and Poisson's ratio of .3 was assumed because material was stainless steel 316L. Free-Free boundary conditions were used on all the surfaces to match the experimental setup.

Table 2: Material Property

Group	Modulus of Elasticity (GPa)	Poisson's Ratio	Density (kg/m^3)
A	2.457	.3	7923
B	2.451	.3	7871
C	2.464	.3	7781

In COMSOL the simulation module used was the frequency domain. The frequency domain analysis provides the full frequency response of the sample when subjected by a harmonic force, within a given frequency range. This experimental setup matches closely with the NDT-RAM experimental setup described previously. The frequency range chosen was 0Khz-85kHz, which closely resembles the frequency range of interest based on the RUS results. A 1N point load is applied in all three directions on the top surface at one end of the sample. This is shown in Figure 12. The total displacement history of the sample is recorded at the other end of the sample.

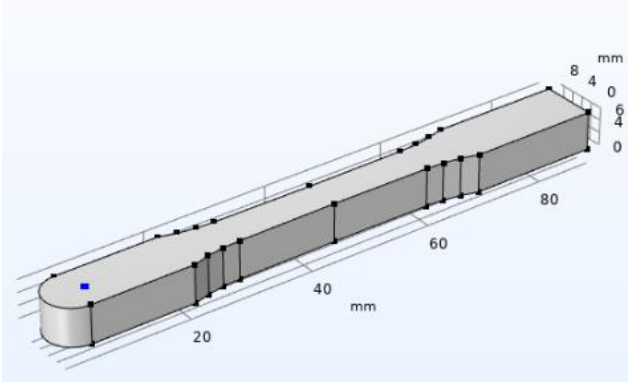

Figure 12: Experimental COMSOL Setup

Chapter 3

MECHANICAL TESTING RESULTS

3.1 Density Evaluation

As previously mentioned, 11 samples from each group were measured and the averages of each group were taken. The results from the density measurements are shown in Figure 13. Based on the results, the change in process parameters affected the structural integrity of the sample. There is a clear difference between the 3 non-heat-treated groups. The density value decreases from around 7925kg/m^3 to 7775kg/m^3. The optimal group (A) has the highest density value, while the lowest values were from the defected groups. Group C had a lot lower density value compared to Group B. For the B group the density dropped about 1 %, while Group C had around a 2 % reduction from optimal group A. Both were manufactured with less than optimal, group B with the lower laser power and Group C with the lower scan speed. The change in scan speed had a greater effect on the part quality and potentially produced more porosity in the samples than reducing the laser power. A potential reason for this is that lowering the scan speed increases the cooling rate of sample, which increases the growth of dendrites[39], thus introducing more porosity in the sample.

Table 5: Density Values

Group	Density(kg/m^3)
A	7922.7
B	7870.9
C	7781.4

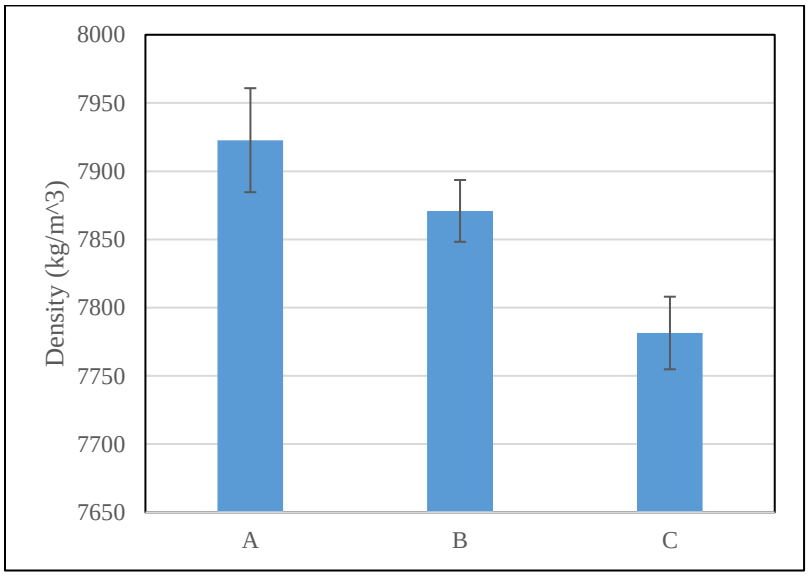

Figure 13: Density Values of Non-HT Groups

3.2 Tensile Testing

The effects of process parameter changes and post-processing heat treatment on the tensile strength, yield strength, and ductility of the manufactured parts were evaluated via tensile stress-strain curves. shows the average stress and strain curve for each group. The stress was calculated by dividing the force by the cross-sectional area which was 36mm^2. The averages

were taken from each group and plotted in the bar graphs in Figure 15. The yield strength was determined using the .2 percent offset method.

For the non-heat-treated groups there were some differences between the UTS, yield, and strain. When looking at Figure 15 and comparing the ultimate tensile strength and the yield strength between the 3 groups there is a very minor difference especially in the yield strength values. The difference in yield strength between the groups is only about 3%. Group A had the highest at around 340MPa and Group C the lowest at around 330MPa. As for the ultimate tensile strength, there is a bit more variation. Group B had the highest ultimate tensile strength at around 570 MPa. This value was higher than the samples printed at optimal condition (Group A), which was 550MPa. Like the yield strength, the percentage difference was not high between the 3 values at around 3%-5%. This was also true for the strain value. The difference between the strain values is less than 3 percent with Group A having the highest strain value of .61. Group C had the lowest strain value at .59.

As for the heat-treated samples, the main difference between the heat treated and non-heat-treated samples were the strain and yield strength. The UTS between the heat-treated groups and non-heat treated were close with one another. Although there was a reduction in the UTS it was only slight and the heat treat had little to no effect. It was found that the heat-treated yield strength values were about 96-98% percent of the non-heat-treated samples. Whereas for the strain and yield values there was more of a difference. Like the UTS values, the yield strength of the heat-treated samples decreased. The range of the yield strength values of the non- heat-treated groups was from about 330-345MPa and the heat -treated group was from 295-310MPa. On average there was roughly a 15 percent reduction in yield strength, due to the heat treatment process. The strain was the only property that increased. Due to the annealing process the

samples strain increased about 15 percent for A and B group. For Group C the strain was the highest at about .78 and its strain increased by about 25 percent.

Table 6: Avg UTS, Yield, and Strain values for each group

Group	Yield (MPa)	UTS	Strain (%)
A	343	542	.61
AH	310	539	.71
B	338	570	.60
BH	314	557	.72
C	332	526	.59
CH	293	513	.78

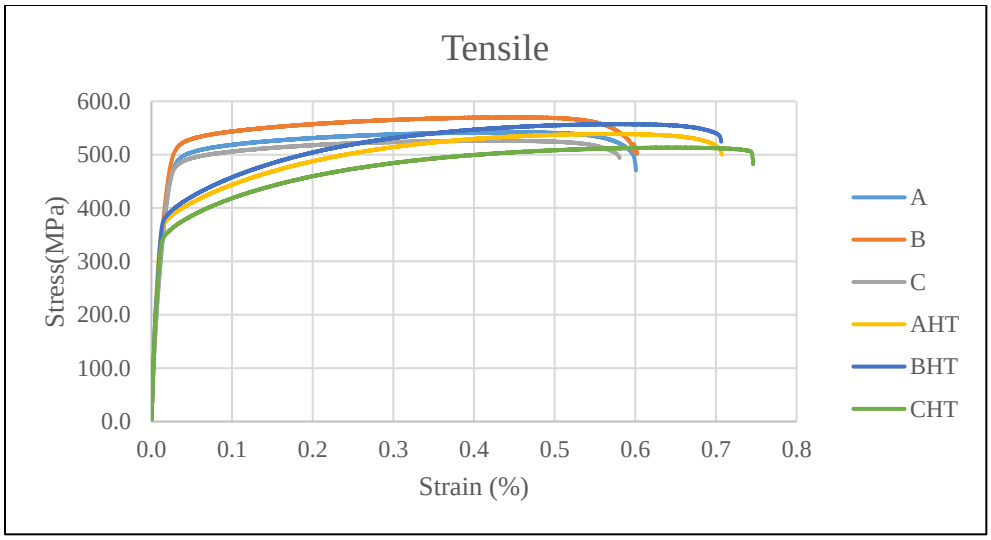

Figure 14 : Stress vs Strain Curve

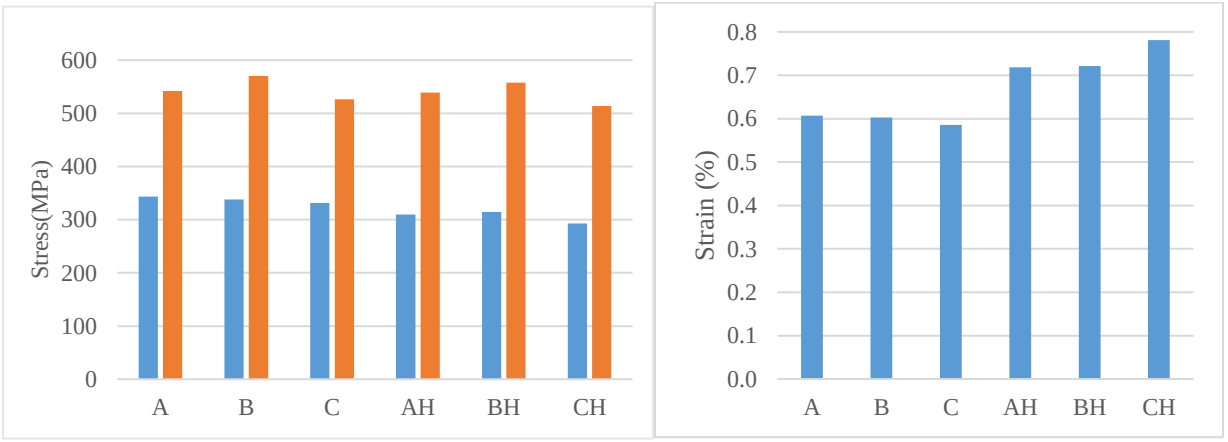

Figure 15: a) Average Yield and UTS Values b) Average strain values

3.3 Fatigue Test

The fatigue data for high cycle and low-cycle analysis are shown in Figure 16. Unlike the tensile test of the non-heat-treated samples, there were more variations between the control group A and the defected group. The defected groups (B and C) show a higher fatigue life at every stress level compared to the optimized group. There was a 25-40 percent increase in fatigue life, based on the change of process parameters. The results from the fatigue test were unexpected.

Lowering the laser power and the scan speed, were originally thought to lower the fatigue life of the sample, due to the increase in defects. These defects were thought to act as crack initiators thus lowering the life, but this was not the case. In conclusion, other factors may have led to lower-than-expected fatigue life in the optimal group.

The fatigue life results from the heat treatment, depict an increase in fatigue life at for stress value under 300 MPa. At stress level 300MPa and 250MPa, the fatigue life nearly doubled and tripled for all the samples. Like the non-heat-treated samples the optimized group had a sub optimal fatigue life compared to the defected group. At stress level 400 MPa the heat-treated samples performed worse on average, compared to non-heat-treated samples. This could be attributed to the reduction in yield strength of the heat-treated samples, causing lower life at the specific stress level. All the samples failed at or below 100,000 cycles.

Table 7: Avg Fatigue Life Values at each cycle for each group

Group	Cycles	Stress (MPa)	Cycles	Stress (MPa)	Cycles	Stress (MPa)
A	100818	400	232052	300	444500	250
B	133872	400	288817	300	765077	250
C	129569	400	342376	300	645750	250
AH	82020	400	373111	300	2100000	250
BH	108815	400	647224	300	2435000	250
CH	55817	400	458722	300	1576000	250

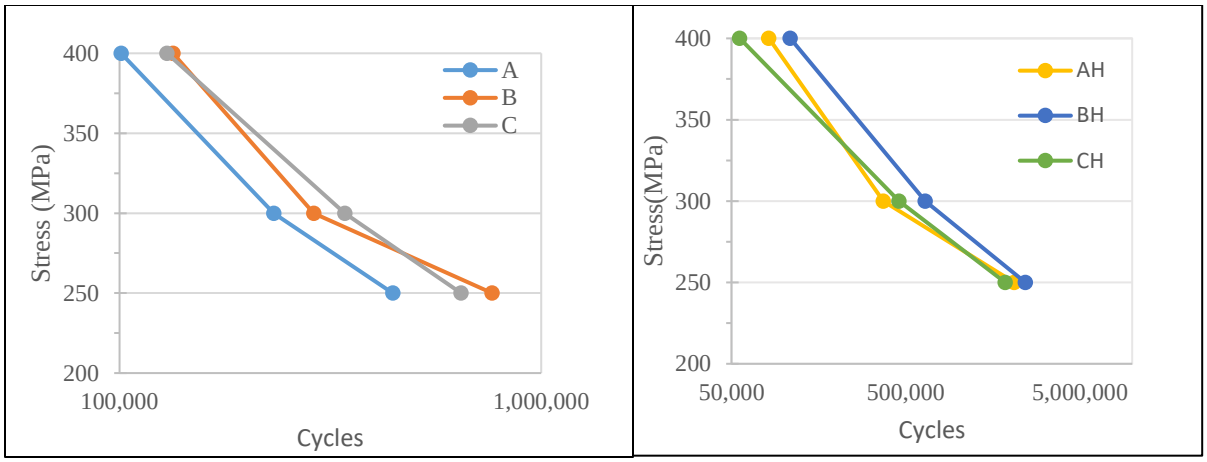

Figure 16: S- N Curves of the Non-HT groups and HT groups.

3.4 Nanoindentation

The nanoindentation hardness and the young modulus of all the samples were measured. Table 8 and Figure 177 show the summary of these results for each group. As can be seen from the results of the non-heat-treated group, there was a slight increase in hardness, because of the change in process parameters. Group A had the lowest hardness value at 4.31GPa, while group C had the highest value at 4.66GPa. The change in laser scan speed resulted in almost a 10 percent increase in hardness. For the modulus values, there was little variation. The max difference between the 3 groups was only around a 1GPa difference. Group B had the lowest modulus at 245GPa, and group C had the highest at 246.4GPa. The change in process parameters did not affect this value too much.

As for the heat-treated samples, there was a reduction in both the hardness and the modulus. The hardness had decreased about 10-20 %, because of the heat treatment process. The samples had become softer. This is also true for the modulus. The modulus for all the samples had decreased, which is consistent with the strain values from the tensile test. Due to the annealing the ductility increased, thus making the material more flexible and less stiff.

Table 8: Nanoindentation Results

Group	**Young Modulus (GPa)**	**Hardness (GPa)**
A	245.7	4.31
B	245.1	4.52
C	246.4	4.66
AH	244.1	3.91
BH	233.7	4.12
CH	238.4	3.69

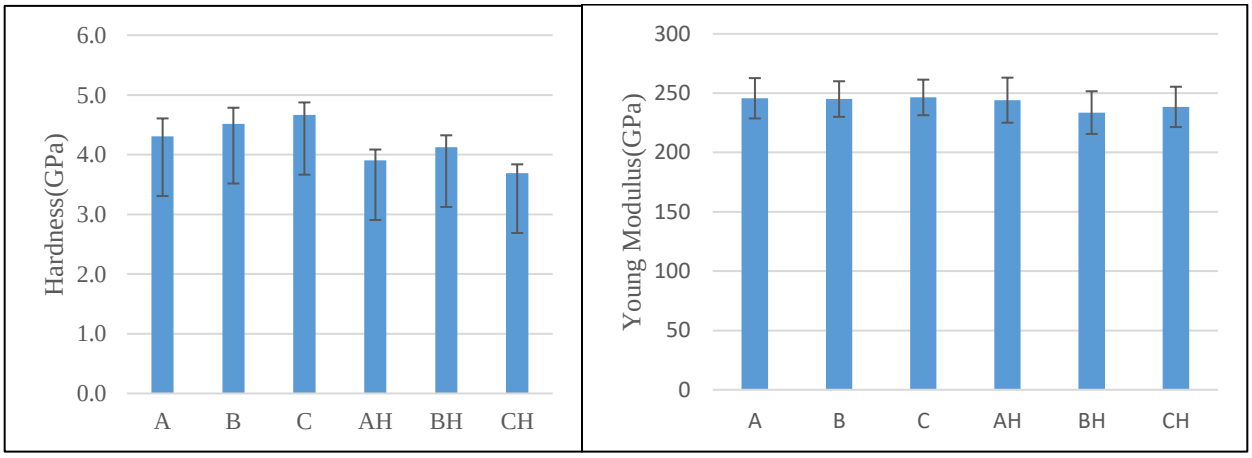

Figure 17: Nanoindentation Results for the Non-HT and HT Groups.

3.5 Correlation Study

A correlation study was conducted to establish a relationship between the non-heat-treated process parameters (laser power and scan speed) and the mechanical properties. Manufacturing process parameters have been shown to change the mechanical properties of a material and by analyzing this relationship manufactures can determine which process has the most effect on certain properties. For example, in Gockel et al study, they investigated the

process-structure relationship between AM process parameters on surface roughness and its effect on the fatigue life of samples. They found that the Sv value had more of a correlation than the Sa value on a structures' fatigue life [40]. This established relationship can possibly help build a framework that can give future insight into how a material might perform, which was showcased in Yan et al study[41]. They created a framework that predicts fatigue life based on the material property and process conditions.

The type of correlation used in this study was the Pearson's correlation which was used to establish the relationship between the process and property of a material. Pearsons's correlation provides an easy way to interpret the strength of the relationship between two variables. This study measures the strength and the direction of the two variables between a value of -1 and 1. These numbers are represented by the value r. The closer the r variable is to -1 or 1 indicates how strongly correlated the two variables are and the + or – indicates the direction. This study was used to correlate each variable to one another and is shown in the heat map in Figure.

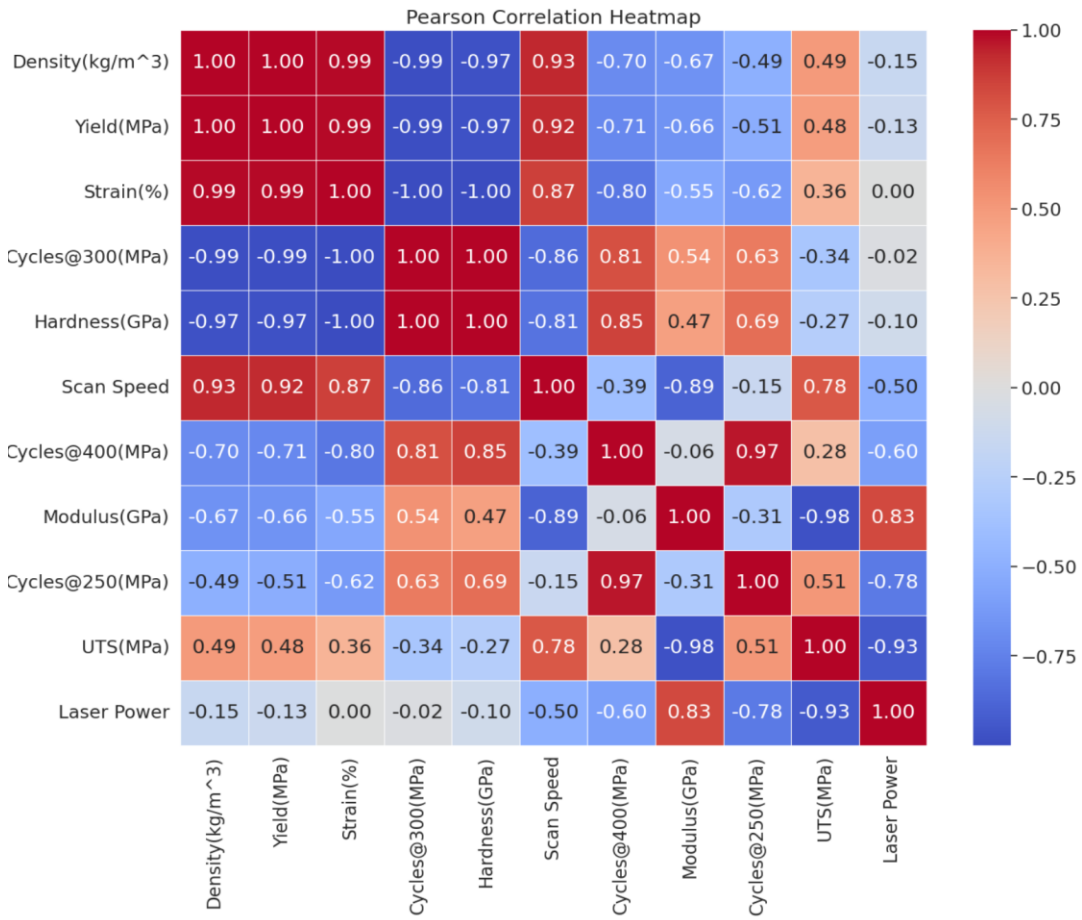

Figure 18: Pearson Correlation heatmap of all the variables.

Looking at the correlation results between our process parameters (laser power and scan speed) and our dependent variables (RUS and mechanical testing), the scan speed had a more consistent stronger relationship to our response variables. The scan speed seems to have a greater effect on the certain mechanical properties of the material (density, yield, strain, hardness, modulus), than the laser power in this study. Density, yield, strain, had a positive relationship with the scan speed, meaning there is a direct correlation between the variables. As the scan speed increases or decreases these outputs will follow in that same direction. For the fatigue results (cycles at 250,300,400), hardness, z-score(mean) and modulus there was a negative correlation meaning that there is an indirect correlation between the variables. The laser power

had a strong positive correlation with the z-score(mean) and the modulus. At certain fatigue levels(250(MPa),400(MPa)), and the UTS had a strong negative correlation. For the other response variables (hardness, yield, density, strain, cycles at 300(MPa)), the laser power had a very weak relationship, because these coefficients are less than .25.

Chapter 4

RUS RESULTS

4.1 RUS Testing

Three main variables affect the resonance of a sample: mass, modulus, and damping. Any change in these variables in a sample due to either process parameter changes or defects will alter the frequency spectrum of the part. These changes can either be shift in resonance frequency, amplitude response, or number of harmonics. Since the change in process parameters and heat treatment will affect the quality of the part it is expected to cause shifts in the resonance frequencies of the part. These shifts in frequency are useful in differentiating parts from one another. The results of the RUS testing are discussed between the groups with different process parameters as well as the ability of RUS to detect heat-treated from non-heat-treated samples will be discussed as well.

Due to variation between the manufacturing process of the samples, it is expected that the resonance frequency of the parts be different between the 3 groups. Accordingly, Figure 19 shows the normalized amplitude RUS test results for the non-heat-treated groups. As can be seen from the figures, the first 9 peaks(-3KHz-35Khz) were relatively similar between each group. However, from beyond this range at the higher frequencies is where most of the frequencies shift occur. The changing process parameters led to shift in the frequencies to the left or to the right

depending on frequency range analyzed. It also caused a change in the amplitude of the resonance peaks, but this was deemed negligible, because the force at which the modal hammer was taps the sample was not consistent which can directly influence the response.

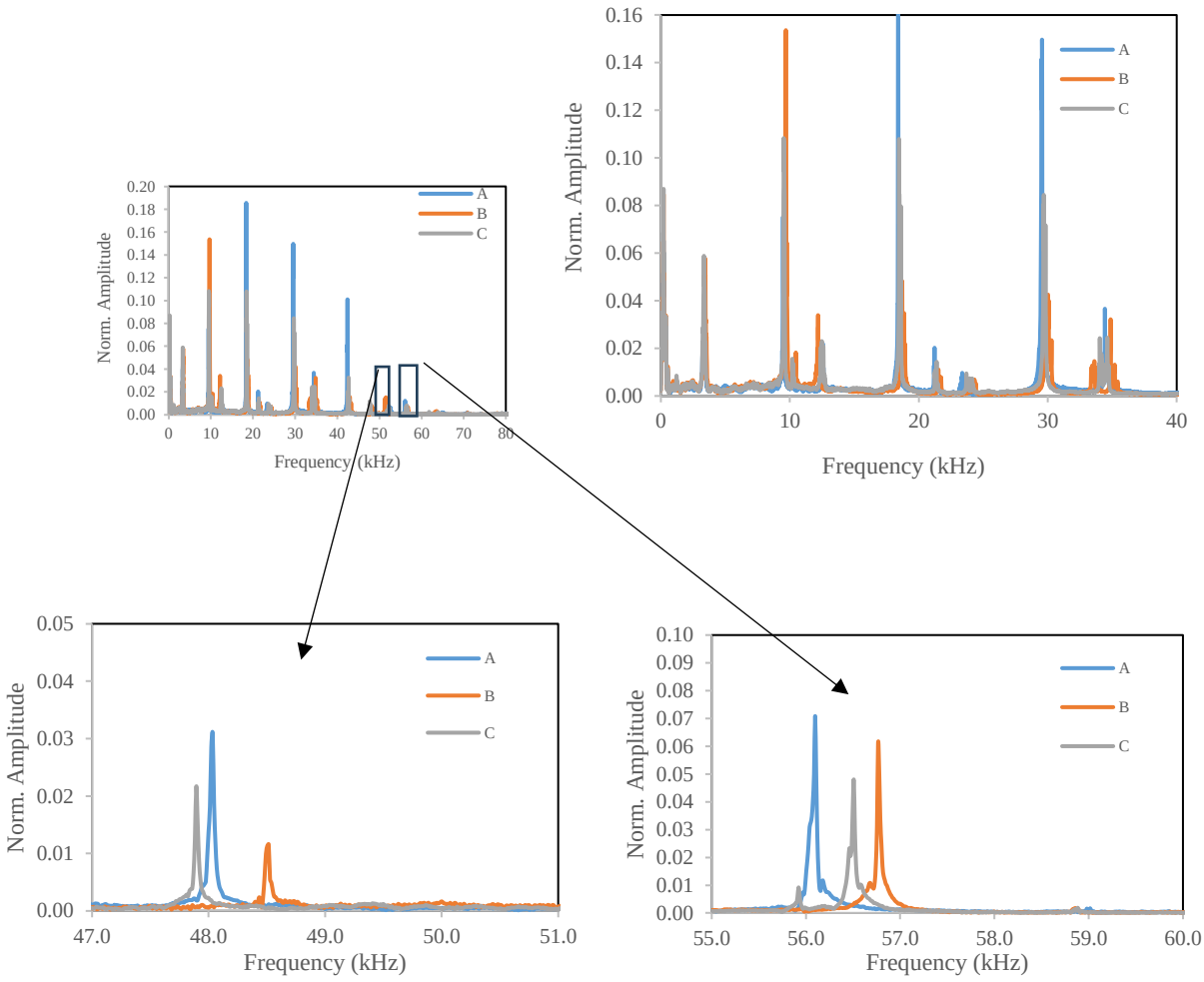

Figure 19: Normalized amplitude frequency spectrum graphs at different frequencies of the non-heat-treated group

Post heat treatment is important in terms of post processing for additive manufactured samples, due to the unwanted defects and porosity that could potentially lower than life mechanical property of a sample. The heat treatment process mainly affects the microstructure of the part. These changes in the microstructure can help improve the quality and mechanical

property of the part depending on the application. Since heat treatment causes a change in the sample's structural integrity it is expected to result in frequency shifts in the samples. Figure 20 shows the frequency spectrum of each group's heat treated sample and non-heat-treated sample. As can be seen from the graphs, most of the frequency shifts occur in the mid to high frequency ranges and there was little deviation in the first few frequencies. The heat treatment caused most of the frequencies to shift to the right (higher frequencies)

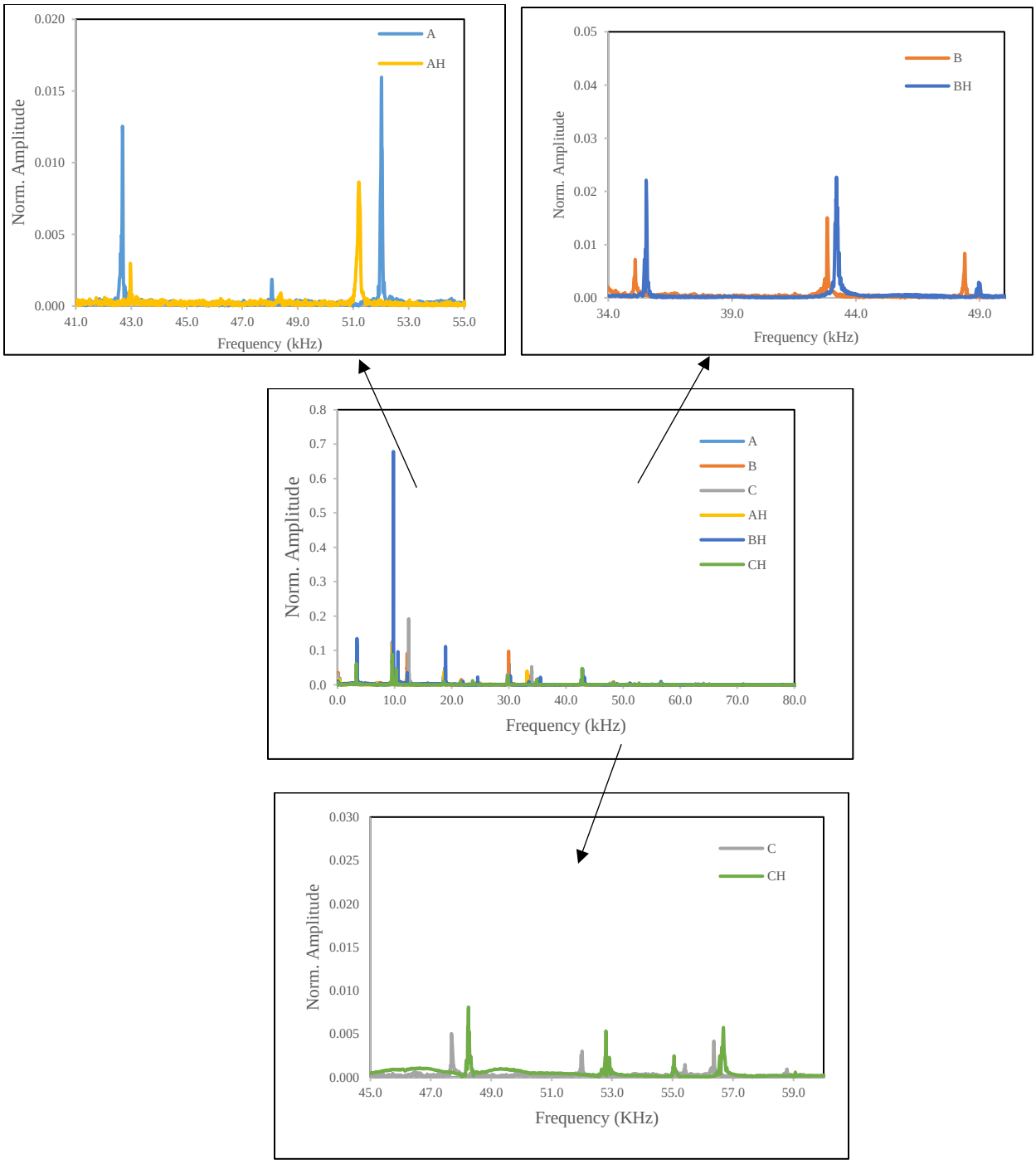

Figure 20: Effect of heat treatment on resonance frequencies between non heat treated and heat-treated groups.

Although the RUS test provides reliable data in showing the difference between one group of samples to another, Z-score provides another very useful statistical way to analyze the frequency response of the sample. The Z-score is a type of statistical analysis that measures the

location of a part's condition within a population, mean, in units of the population standard deviation. The normal z-score is calculated as (population average/ population standard deviation). The median absolute deviation or (MAD) z- score is calculated as (population median/population median absolute deviation. Both calculations show a part's location relative to the population. This analysis helps provide insight in part differentiation as well. Parts with smaller variations should have relatively close Z-scores. Whereas parts that have more variations between each other will have greater z-scores in either the positive or negative direction.

The MAD Z score was used in the study to analyze the frequency response of all groups compared to the optimal group A and this is shown in Figure 21. The plot shows a nice and clear separation between the 6 groups. As can be seen from this z-plot, the process parameters (low laser power) from Group B caused an overall frequency shift to the left (lower frequency). For Group C, the process parameter (low scan speed) caused an overall shift in the frequency to the right (higher frequencies). The low laser power had caused a greater variation in part quality than the lower scan speed, based on the z-score mean value results. As for the heat treatment groups, the heat treatment caused an overall frequency shift to the right for all the groups. Groups AH and BH had a greater shift to their corresponding non-heat treatment group, whereas the shifts in the C and CH group were much minor.

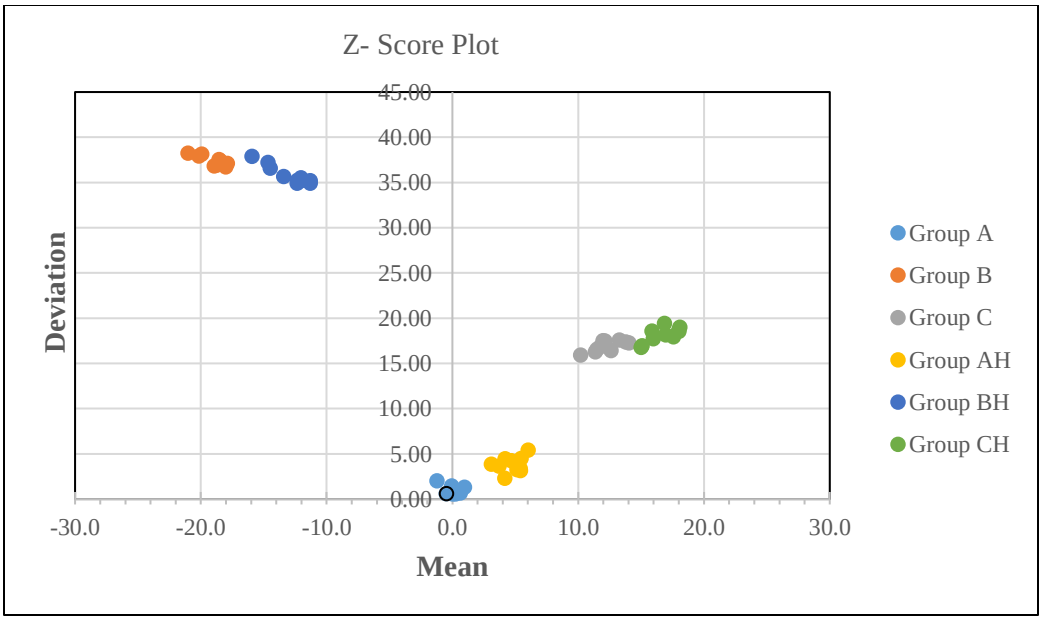

Figure 21: Z- Score Plot graphs for Heat-treated and Non-Heat-treated groups

Based on the frequency spectrum results and the z-scores results, RUS was able to successfully characterize the 6 different sample groups, based on the process parameter condition.

4.2 Correlation Study: RUS and Mechanical Property

A correlation study was also used between the RUS test and the destructive test. A relationship between the Z-scores from the RUS test and the mechanical properties was studied for the non-heat-treated group. The z-scores were used up to the 17th harmonic, to best represent the overall change in the frequency spectrum between the 3 groups. The results of Pearson correlation test are illustrated in the graphs below. Figure 22 shows the correlation between the RUS test and the tensile testing.

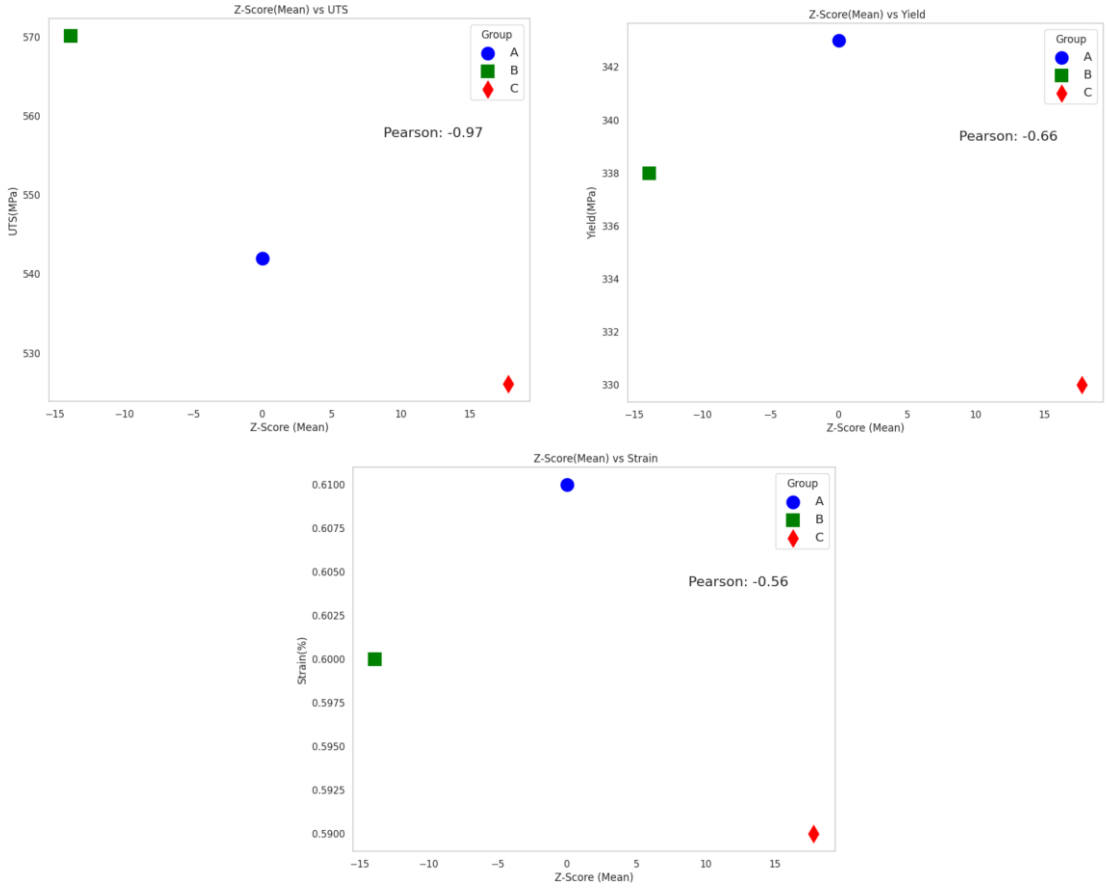

Figure 22: Pearson Correlation between RUS and Tensile Testing

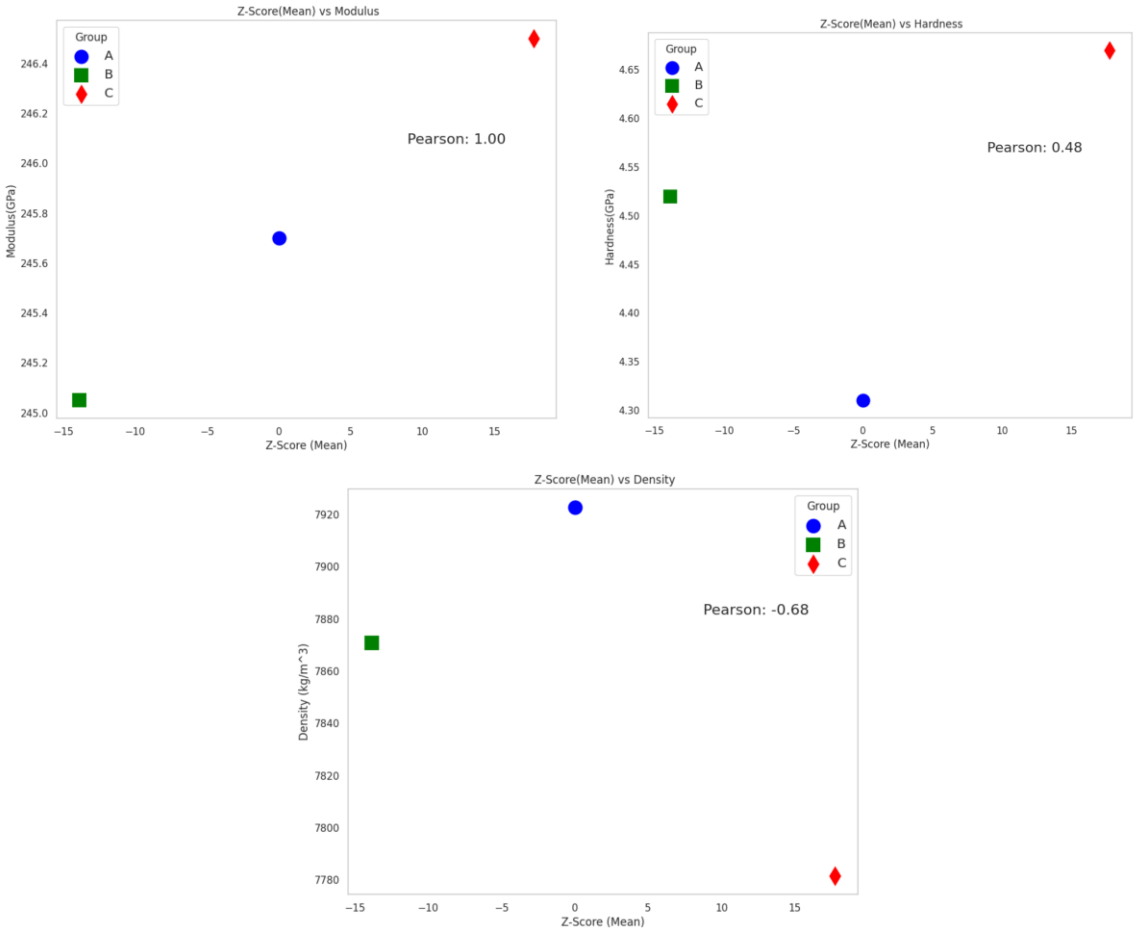

Figure 23:Pearson Correlation between RUS and Nanoindentation/Density

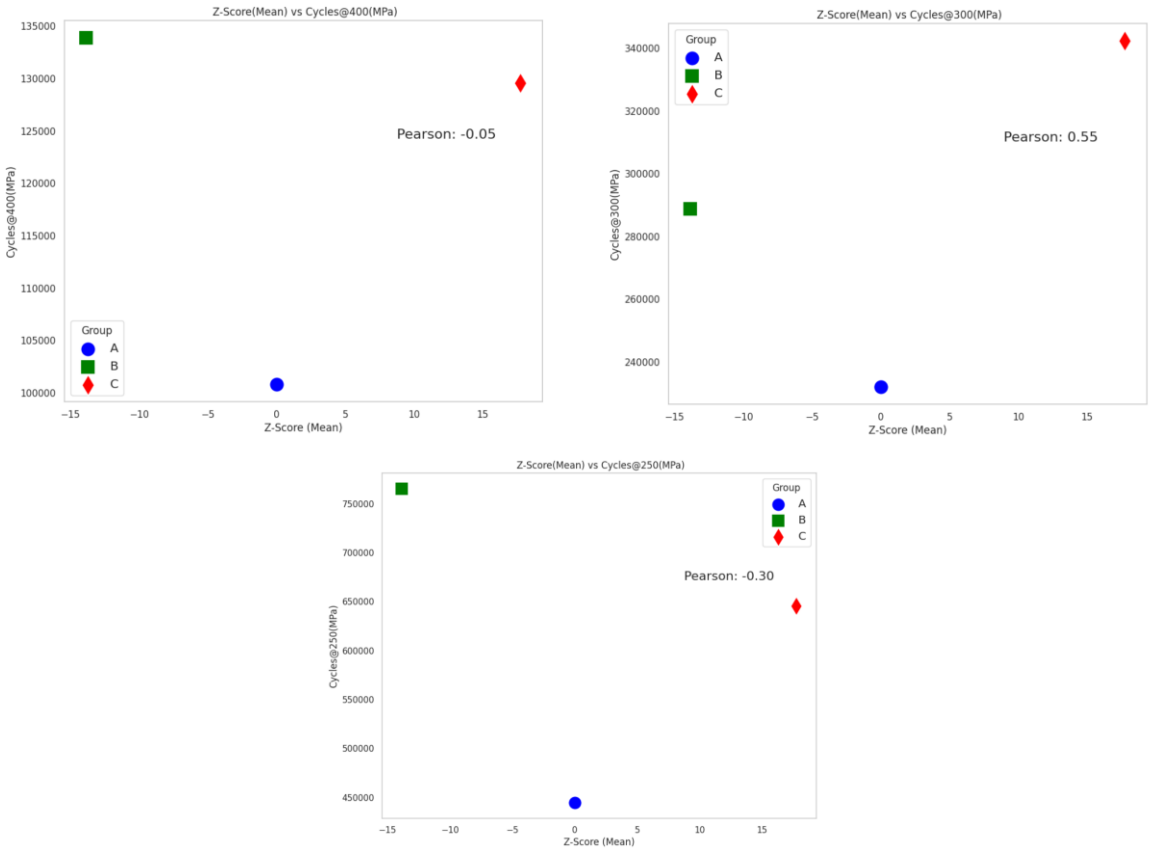

Figure 24: Pearson Correlation between RUS and Fatigue Testing

As can been in the figures, The r value ranges from -.6 to -.96, thus showing a moderate to strong correlation between the two tests. The negative value resulting in an indirectly proportional relationship between the tests. For example, as the z-score increases the tensile properties of the sample will decrease. The density and nanoindentation test show similar a similar relationship with the RUS test. Figure 23 shows the r values of the density, hardness, and modulus. These results show a moderate to very strong correlation, like the tensile test results. The modulus showed a very strong relationship with RUS results, while density had a moderately strong correlation with a value of -.68. These strong relationships are to be expected since these factors are very important properties when determining a parts' resonant frequency[38,42]. The hardness results show a moderate correlation with a r value of .48. Figure

24 shows the correlation between the fatigue test and the RUS test. The correlation values for this test were no correlation to a moderate correlation, based on the stress level being analyzed.

Based on this preliminary study, most of the tests other than the fatigue testing show a moderate to strong correlation with r values above .5. This means that RUS correlates well with the mechanical properties of a given sample. This relationship between these two tests could provide insight into how a material might perform in the future based on the given process parameters.

Chapter 5

FINITE ELEMENT ANALYSIS

5.1 FEA Results

The finite element method was used to generate the frequency spectrum of the three groups, using simulations. The use of simulation provides a way to generate many frequency spectrums for analysis to detect possible defects and location based on the change of mode or frequency shifts. The frequency spectrum generated by FEA will be compared to the RUS results, to assess the feasibility of using FEA in tangent with RUS as a viable option for part qualification.

In COMSOL, the frequency domain analysis was used to provide the full spectrum response of the samples. Figure 25 shows the COMSOL results from the frequency domain study for all groups. As can be seen from the figure, the resonant frequencies are nearly identical between the three groups, until around the higher frequency range from (60kHz-85kHz). At around this range the frequency starts to deviate to the right for groups B and C, with C group having the biggest frequency shift. Whereas for Group B, the resonant frequencies are still very

close to the optimal group A. Meaning that the change in material properties of Group B (density and mass) had very a small effect on the resonant frequencies, when comparing to Group A. The most noticeable difference is in the amplitude response between these three groups.

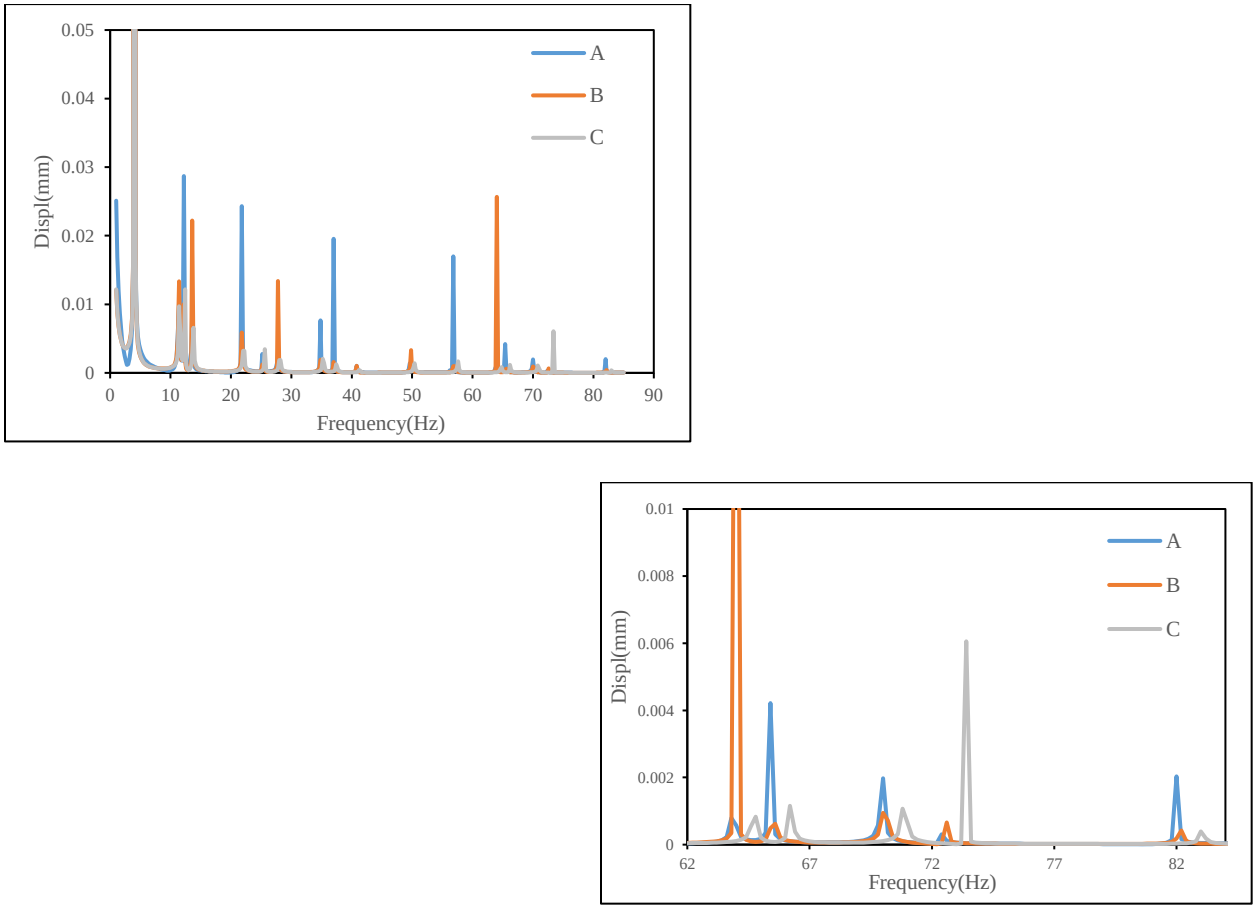

Figure 25: COMSOL Results for groups A, B, and C

5.2 Discussion: Experimental vs FEA simulations

Comparing the experimental to the FEA simulations there are some similarities, but there exist very big differences. For both experiments the major frequency shifts happen at the mid to higher frequencies and both spectrums show a variance between the defected and non-defected groups. The biggest difference is how large the variations in resonant frequencies are. As stated in the previous section the resonance frequencies between the simulated data were very similar for group A and B, with a slight difference in group C at the higher harmonics. This statement is

simply not true for the experimental data which showed large variation differences between these three groups especially at the higher modes of frequencies.

When comparing the simulated results to the experimental results for group A, the results are within a margin of error of about 10 percent. There are very large discrepancies in the first few modes(0-35Khz) and the error is very high at around 20 %. This error starts to dwindle quite a bit and dwindles down to around 4% at the higher frequency ranges (35Khz-85Khz). The results for group A between both experiments are quite reasonable and spectrum analysis match quite well. However, this does not hold true for Groups B and C. For Group B, the frequency spectrum is quite different. Like Group A results the error was quite in the first few modes. However, this stayed true for the mid frequency ranges (35kHz to 50khz). In the RUS results, the frequencies in this middle range were a lot lower than the simulation results. For group C, again the first few modes there were large discrepancies, however this error starts to dwindle down to around 5 percent at the higher ranges. The error for this group was slightly marginable at around 11 percent.

As mentioned earlier the shifts in frequency between the RUS and the COMSOL results are very different. When looking at the resonant frequencies of the RUS results there presented in table .. major frequency shifts between the defected and the non-defected groups. The change in laser power caused a reduction in resonant frequency between the 9^{th} and 14^{th} harmonic and a shift to the higher harmonics in 15^{th} to the 17^{th} harmonic. For Group C RUS results, the change in scan speed caused a shift to the higher frequencies from the 14^{th} to the 17^{th} harmonic. However, the FEA results do not paint the same picture, especially group B's results. The FEA frequency spectrum does not capture the shift in resonance frequency between the 9^{th} and 14^{th} harmonic. Although there is a shift to the right at the higher frequencies the shift is very minor.

Thus, resulting in a higher percentage error compared to Group A and C. The shifts in group C in the FEA results match the RUS results with both showing a frequency shift to the right, but again the shift is not quite as high.

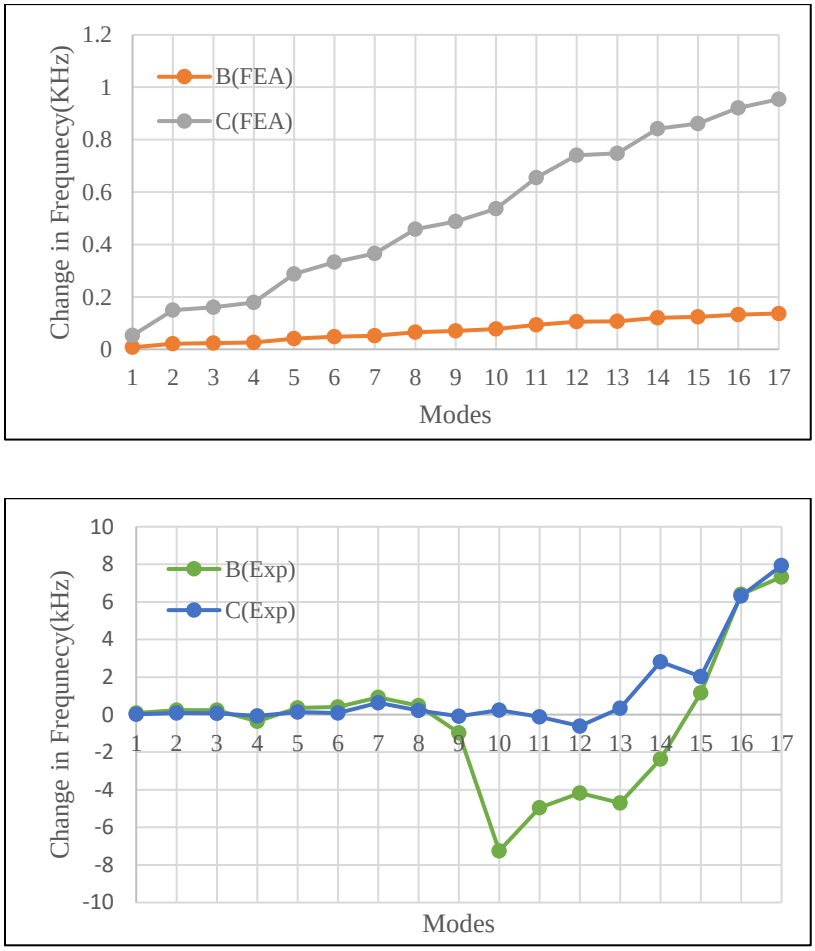

Figure 26: Changes in Frequency at each mode compared to Group A

Chapter 6

CONCLUSION

The goals of this work had many objectives. Samples were made with different process parameters and post-heat treated to study the effects of how these parameters affected the mechanical properties of the sample. Based on the mechanical property results, the different process parameters did influence the material properties. For example, the low laser power or scan speed had either enhanced the properties of the sample or decreased depending on the material property being evaluated. The density and fatigue of the non-heat-treated parts showed the most variation between the process conditions. Whereas the nanoindentation and tensile testing results showed little variation with most of mechanical properties showing less than 3 percent difference between the non-heat-treated parts. Comparing the heat treated and non-heat-treated samples, the heat treat had improved mainly the ductility of the part. This was to be expected, because of the heat treatment process chosen(annealing). The strain had increased significantly, because of the annealing as well as the fatigue life of the samples at stress levels below the yield point.

The second objective of the study was to test RUS ability to characterize the metal AM samples. From the RUS results, it was successful in not only characterizing the non-heat-treated groups, but also the heat-treated groups as well. The frequency spectrum shows that the changes in process parameters affected the resonance peaks in wither shifting the peaks to either the right or left depending on the frequency range being analyzed. The most variation in resonant frequencies occurred in the mid to high frequency ranges. There was little variation in the first about 9 harmonics (3Khz to 30Khz). These unique shifts in frequency are further evaluated using the z-score analysis. From the z-score results, there is a very clear separation between the 6

different samples. Parts with similar manufacturing conditions are tightly clustered together, thus proving RUS ability to characterize the samples.

Once the material properties were ascertained and RUS test finished, a correlation study was used to establish a relationship between the non-heat-treated parts and the mechanical parameters and z-scores. Pearson's correlation was used to study the influence the laser power and scan speed had on the mechanical parameters. Based on the correlation heatmap and corresponding coefficients values, scan speed seemed to have a greater influence of the part for most of the response variables being studied. For the density, yield, strain, hardness, z-score, cycles at 300MPa, modulus, the r values were closer to one in either the positive or negative relationship, meaning a stronger relationship between the variables discussed. Whereas the laser power had a stronger influence on the cycles at 250 and 400 MPa, ultimate tensile strength. Understanding how the different process parameters influence the mechanical properties is of great significance in terms of improving the manufacturing process.

The mechanical properties of the samples and the results from the RUS (Z-scores (Mean), were evaluated to build a correlation between the destructive test and the non-destructive test. Based on these results, there was a strong correlation between the two tests except for the fatigue testing, The r values for these tests were relatively low meaning a weak correlation. For the rest of the mechanical properties, there exist mostly a strong to moderate relationship in either the positive or negative direction. Modulus had a perfect positive linear relationship with the RUS results, meaning these two variables are directly correlated. The findings from these results are promising, in that they can provide explanation in how far the z-score deviates and its' impact on the mechanical properties.

Finally, FEM was used to compare the frequency spectrum of the numerical results to the experimental results. Using the density and modulus from the mechanical testing a digital twin or virtual model was created to show the changes in the frequency spectrum. Using a frequency domain analysis, FEM results were promising in showing a difference between the non-heat-treated groups. At the higher frequency ranges there was a shift in the resonance frequencies, thus proving its ability to show differences. Although there is a promise of using FEA to serve as digital model, when comparing the frequency spectrum to the experimental spectrum there exist discrepancies. Comparing numerical results to the experimental results, Group A (control group) had the least amount of error at 10 percent. For group B and C, the error was slightly higher at around 11-15 percent. When comparing the resonant peaks of these two groups the shifts in the frequency in the experimental are more pronounced, especially for group B. The discrepancies could be from either nonlinear effects or property differences.

The results presented in this thesis are encouraging for RUS to characterize AM parts. Provide a baseline for correlating the RUS results to the mechanical properties and using FEA to further enhance quality testing. Future works, to help improve the validity of what was proved in this thesis are to:

1. Material Testing
    - Manufacture more groups/ samples at different laser power and scan speeds to further evaluate process structure relationship.
    - Have more samples in each group for mechanical testing for stronger statistical analysis conclusions

2. Numerical Analysis

    - In material modeling consider anisotropy of the sample for more accurate results

References

[1] Korner, M. E. H., Lambán, M. P., Albajez, J. A., Santolaria, J., Corrales, L. D. C. N., and Royo, J., 2020, "Systematic Literature Review: Integration of Additive Manufacturing and Industry 4.0," Metals (Basel), **10**(8), pp. 1–24.

[2] Chadha, K., Tian, Y., Spray, J. G., and Aranas, C., 2020, "Effect of Annealing Heat Treatment on the Microstructural Evolution and Mechanical Properties of Hot Isostatic Pressed 316L Stainless Steel Fabricated by Laser Powder Bed Fusion," Metals (Basel), **10**(6), pp. 1–18.

[3] Tucho, W. M., Lysne, V. H., Austbø, H., Sjolyst-Kverneland, A., and Hansen, V., 2018, "Investigation of Effects of Process Parameters on Microstructure and Hardness of SLM Manufactured SS316L," J Alloys Compd, **740**, pp. 910–925.

[4] Liverani, E., Toschi, S., Ceschini, L., and Fortunato, A., 2017, "Effect of Selective Laser Melting (SLM) Process Parameters on Microstructure and Mechanical Properties of 316L Austenitic Stainless Steel," J Mater Process Technol, **249**, pp. 255–263.

[5] Kudzal, A., McWilliams, B., Hofmeister, C., Kellogg, F., Yu, J., Taggart-Scarff, J., and Liang, J., 2017, "Effect of Scan Pattern on the Microstructure and Mechanical Properties of Powder Bed Fusion Additive Manufactured 17-4 Stainless Steel," Mater Des, **133**, pp. 205–215.

[6] Seifi, M., Gorelik, M., Waller, J., Hrabe, N., Shamsaei, N., Daniewicz, S., and Lewandowski, J. J., 2017, "Progress Towards Metal Additive Manufacturing Standardization to Support Qualification and Certification," JOM, **69**(3), pp. 439–455.

[7] Thompson, A., Maskery, I., and Leach, R. K., 2016, "X-Ray Computed Tomography for Additive Manufacturing: A Review," Meas Sci Technol, **27**(7).

[8] Honarvar, F., and Varvani-Farahani, A., 2020, "A Review of Ultrasonic Testing Applications in Additive Manufacturing: Defect Evaluation, Material Characterization, and Process Control," Ultrasonics, **108**.

[9] Segovia Ramírez, I., García Márquez, F. P., and Papaelias, M., 2023, "Review on Additive Manufacturing and Non-Destructive Testing," J Manuf Syst, **66**, pp. 260–286.

[10] Migliori, A., Sarrao, J. L., Visscher, W. M., Bell, T. M., Lei, M., Fisk, Z., and Leisure, R. G., 1993, "Resonant Ultrasound Spectroscopic Techniques for Measurement of the Elastic Moduli of Solids," Physica B Condens Matter, **183**(1–2), pp. 1–24.

[11] *Resonant Ultrasound Spectroscopy*.

[12] Li, G., and Gladden, J. R., 2010, "High Temperature Resonant Ultrasound Spectroscopy: A Review," Int J Spectrosc, **2010**, pp. 1–13.

[13] Longo, R., Delaunay, T., Laux, D., El Mouridi, M., Arnould, O., and Le Clézio, E., 2012, "Wood Elastic Characterization from a Single Sample by Resonant Ultrasound Spectroscopy," Ultrasonics, **52**(8), pp. 971–974.

[14] Cai, X., Peralta, L., Brenner, R., Iori, G., Cassereau, D., Raum, K., Laugier, P., and Grimal, Q., 2020, "Anisotropic Elastic Properties of Human Cortical Bone Tissue Inferred from Inverse Homogenization and Resonant Ultrasound Spectroscopy," Materialia (Oxf), **11**.

[15] Niu, H., Fan, F., Wang, R., Zhang, Q., Shen, F., Ren, P., Liu, T., Fan, Y., and Laugier, P., 2019, "Elastic Properties Measurement of Human Enamel Based on Resonant Ultrasound Spectroscopy," J Mech Behav Biomed Mater, **89**, pp. 48–53.

[16] Davis, E. S., Sturtevant, B. T., Sinha, D. N., and Pantea, C., 2016, "Resonant Ultrasound Spectroscopy Studies of Berea Sandstone at High Temperature," J Geophys Res Solid Earth, **121**(9), pp. 6401–6410.

[17] Whitney, T. M., Green, R. E., and Centerfor, J., 1996, *Low Temperature Characterization of Carbon Epoxy Composites: An Application of Resonant Ultrasound Spectroscopy*.

[18] Lee, Y. S., and Chung, M. J., 2000, "A Study on Crack Detection Using Eigenfrequency Test Data," Comput Struct, **77**(3), pp. 327–342.

[19] Kam, T. Y., and Lee, T. Y., 1992, "Detection of Cracks in Structures Using Modal Test Data," Eng Fract Mech, **42**(2), pp. 381–387.

[20] Flynn, K., and Radovic, M., 2011, "Evaluation of Defects in Materials Using Resonant Ultrasound Spectroscopy," J Mater Sci, **46**(8), pp. 2548–2556.

[21] du Plessis, A., Yadroitsava, I., and Yadroitsev, I., 2020, "Effects of Defects on Mechanical Properties in Metal Additive Manufacturing: A Review Focusing on X-Ray Tomography Insights," Mater Des, **187**.

[22] Kim, F. H., Moylan, S. P., Garboczi, E. J., and Slotwinski, J. A., 2017, "Investigation of Pore Structure in Cobalt Chrome Additively Manufactured Parts Using X-Ray Computed Tomography and Three-Dimensional Image Analysis," Addit Manuf, **17**, pp. 23–38.

[23] Rossin, J., Goodlet, B., Torbet, C., Musinski, W., Cox, M., Miller, J., Groeber, M., Mayes, A., Biedermann, E., Smith, S., Daly, S., and Pollock, T., 2020, "Assessment of Grain Structure Evolution with Resonant Ultrasound Spectroscopy in Additively Manufactured Nickel Alloys," Mater Charact, **167**.

[24] Dababneh, F., and Taheri, H., 2022, "Investigation of the Influence of Process Interruption on Mechanical Properties of Metal Additive Manufacturing Parts," CIRP J Manuf Sci Technol, **38**, pp. 706–716.

[25] Taheri, H., Williams, C., Krenek, R., Weaver, G., and Taheri, M., *Proceedings of the ASME 2022 International Mechanical Engineering Congress and Exposition IMECE2022*.

[26] Ibrahim, Y., Li, Z., Davies, C. M., Maharaj, C., Dear, J. P., and Hooper, P. A., 2018, "Acoustic Resonance Testing of Additive Manufactured Lattice Structures," Addit Manuf, **24**, pp. 566–576.

[27] McGuigan, S., Arguelles, A. P., Obaton, A. F., Donmez, A. M., Riviere, J., and Shokouhi, P., 2021, "Resonant Ultrasound Spectroscopy for Quality Control of Geometrically Complex Additively Manufactured Components," Addit Manuf, **39**.

[28] Obaton, A.-F., Wang, Y., Butsch, B., and Huang, & Q., "A Non-Destructive Resonant Acoustic Testing and Defect Classification of Additively Manufactured Lattice Structures."

[29] Obaton, A. F., Fallahi, N., Tanich, A., Lafon, L. F., and Weaver, G., 2024, "Statistical Analysis and Automation Through Machine Learning of Resonant Ultrasound Spectroscopy Data from Tests Performed on Complex Additively Manufactured Parts," J Nondestr Eval, **43**(1).

[30] Todd, M. A., Hunt, J., and Todd, I., 2019, "Investigation into Using Resonant Frequency Measurements to Predict the Mechanical Properties of Ti-6Al-4V Manufactured by Selective Laser Melting," Sci Rep, **9**(1).

[31] Greco, S., Gutzeit, K., Hotz, H., Kirsch, B., and Aurich, J. C., 2020, "Selective Laser Melting (SLM) of AISI 316L—Impact of Laser Power, Layer Thickness, and Hatch Spacing on Roughness, Density, and Microhardness at Constant Input Energy Density," International Journal of Advanced Manufacturing Technology, **108**(5–6), pp. 1551–1562.

[32] Guo, W., Feng, B., Yang, Y., Ren, Y., Liu, Y., Yang, H., Yang, Q., Cui, L., Tong, X., and Hao, S., 2022, "Effect of Laser Scanning Speed on the Microstructure, Phase Transformation and Mechanical Property of NiTi Alloys Fabricated by LPBF," Mater Des, **215**.

[33] Beardslee, L. B., Remillieux, M. C., and Ulrich, T. J., 2021, "Determining Material Properties of Components with Complex Shapes Using Resonant Ultrasound Spectroscopy," Applied Acoustics, **178**.

[34] Ronneberg, T., Davies, C. M., and Hooper, P. A., 2020, "Revealing Relationships between Porosity, Microstructure and Mechanical Properties of Laser Powder Bed Fusion 316L Stainless Steel through Heat Treatment," Mater Des, **189**.

[35] Chadha, K., Tian, Y., Spray, J. G., and Aranas, C., 2020, "Effect of Annealing Heat Treatment on the Microstructural Evolution and Mechanical Properties of Hot Isostatic Pressed 316L Stainless Steel Fabricated by Laser Powder Bed Fusion," Metals (Basel), **10**(6), pp. 1–18.

[36] Diniță, A., Neacșa, A., Portoacă, A. I., Tănase, M., Ilinca, C. N., and Ramadan, I. N., 2023, "Additive Manufacturing Post-Processing Treatments, a Review with Emphasis on Mechanical Characteristics," Materials, **16**(13).

[37] Ura-Bińczyk, E., Dobkowska, A., Bazarnik, P., Ciftci, J., Krawczyńska, A., Chromiński, W., Wejrzanowski, T., Molak, R., Sitek, R., Płociński, T., Jaroszewicz, J., and Mizera, J., 2022, "Effect of Annealing on the Mechanical and Corrosion Properties of 316L Stainless Steel Manufactured by Laser Powder Bed Fusion," Materials Science and Engineering A, **860**.

[38] Taheri, H., Dababneh, F., Weaver, G., and Butsch, B., 2022, "Assessment of Material Property Variations with Resonant Ultrasound Spectroscopy (RUS) When Using Additive Manufacturing to Print over Existing Parts," Journal of Advanced Joining Processes, **5**.

[39] Larimian, T., Kannan, M., Grzesiak, D., AlMangour, B., and Borkar, T., 2020, "Effect of Energy Density and Scanning Strategy on Densification, Microstructure and Mechanical Properties of 316L Stainless Steel Processed via Selective Laser Melting," Materials Science and Engineering: A, **770**.

[40] Yan, W., Lin, S., Kafka, O. L., Yu, C., Liu, Z., Lian, Y., Wolff, S., Cao, J., Wagner, G. J., and Liu, W. K., 2018, "Modeling Process-Structure-Property Relationships for Additive Manufacturing," Frontiers of Mechanical Engineering, **13**(4), pp. 482–492.

[41] Yan, W., Lian, Y., Yu, C., Kafka, O. L., Liu, Z., Liu, W. K., and Wagner, G. J., 2018, "An Integrated Process–Structure–Property Modeling Framework for Additive Manufacturing," Comput Methods Appl Mech Eng, **339**, pp. 184–204.

[42] Le Bourdais, F., Rathore, J. S., Ly, C., Pellat, M., Vienne, C., Bonnefoy, V., Bergeaud, V., and Garandet, J. P., 2022, "On the Potential of Resonant Ultrasound Spectroscopy Applied to the Non-Destructive Characterization of the Density of (LPBF) Additively Manufactured Materials," Addit Manuf, **58**.